Structural Chemistry
https://doi.org/10.1007/s11224-022-02063-2

ORIGINAL RESEARCH

Size-dependent adsorption performance of ZnO nanoclusters for drug delivery applications

Mustafa Kurban[1] · **İskender Muz**[2]

Received: 10 May 2022 / Accepted: 18 September 2022

Abstract

We have investigated the size-dependent adsorption performance of ZnO nanoclusters (NCs) as drug delivery carriers for the first time. Our results show that the adsorption energy of the favipiravir drug on the ZnO NCs is predicted in the range of − 26.69 and − 34.27 kcal/mol. The adsorption energy (− 34.27 kcal/mol) between $(ZnO)_{18}$ NC and the favipiravir is energetically desirable and more favorable than the other interactions. The size of ZnO NCs and the position of the favipiravir on the ZnO NCs cause a decrease in the energy gap, which makes the charge-transfer process easier. The bonds between O–Zn, N–Zn, and F–Zn atoms exhibit dual covalent and ionic natures. The non-covalent interaction analysis shows that the strongest H-bonds are observed near NH_2 within the favipiravir molecule. Finally, the acquired results show that the interaction of ZnO NCs with the favipiravir anticancer drug can have the potential as drug delivery carriers.

Keywords ZnO nanoclusters · Favipiravir · Adsorption · DFT · Drug delivery

Introduction

The bulk zinc oxide (ZnO) and its different forms as nanostructure (nanoparticles, nanowires, nanotubes, etc.) have attracted great scrutiny in many areas including solar cells, light-emitting/detecting diodes, and gas sensors [1–9]. ZnO nanoparticles (NPs)/quantum dots (QDs), more specifically, have been significant attention because of their desirable properties such as strong adsorption capability and easily tunable surface used in important areas such as photosensors [10], electronics [11], and biomedical applications [12]. The use of ZnO NPs in biomedicine enables the treatment of different diseases such as bacterial, viral, and carcinogenic due to their remarkable properties such as biocompatibilities, their low cost, biosafety, low toxicity, and heat resistivity in comparison to other metal oxide NPs, which make them suitable for drug delivery systems [13, 14]. Also, ZnO NPs can display inherent anticancer and antimicrobial activities which make them more excellent than other commonly used drug carriers, such as lipid and polymeric NPs [15]. Several reports address the interaction and adsorption behavior of ZnO NPs and nanoclusters (NCs) with different systems [16–21]. The interactions of $Zn_{12}O_{12}$ NC with 6-thioguanine anticancer drug show that $Zn_{12}O_{12}$ NC can have the potential as drug delivery carriers [22].

Many treatments including oral and injection medicines can adversely affect healthy cells and cause side and toxic effects [23]. In some cases, furthermore, it can be possible to use higher doses of a drug to get rid of the effect of the disease [24]. Recent studies show that nanotechnology plays a significant role as drug delivery carrier [25] and has always made it easy to control drug release characteristics of time course and/or location in the body [26, 27]. Most

✉ Mustafa Kurban
mkurbanphys@gmail.com

✉ İskender Muz
iskendermuz@yahoo.com

[1] Department of Electrical and Electronics Engineering, Kırşehir Ahi Evran University, 40100 Kırşehir, Turkey

[2] Department of Mathematics and Science Education, Nevşehir Hacı Bektaş Veli University, 50300 Nevşehir, Turkey

Published online: 30 September 2022

importantly, drug delivery systems can deliver a rather high amount of drug molecules and reduce possible severe side effects without producing a toxic effect [28].

Favipiravir has shown efficacy against many RNA viruses [29], but the reported side effects [30] arising during favipiravir treatment have an important place for patients. In this context, it is significant to reduce adverse side and toxic effects of treatment to healthy cells, so ZnO NCs are designed as drug delivery systems for favipiravir treatment. The literature survey showed that ZnO NC has a potential in drug-carrying systems [31].

In this context, the main objective of this study was to clarify the potential mechanism of possible interaction between ZnO NCs with different sizes and favipiravir anticancer drug and to figure out the potential use of ZnO NCs as a drug carrier. Herein, the electronic and energetic properties such as the adsorption energy, binding energy, density of states, and UV–vis spectra were performed using density functional theory (DFT) and time-dependent DFT.

Computational details

The DFT simulations were implemented to understand the interaction mechanisms of the favipiravir drug molecule with ZnO NCs (with different sizes) along with B3LYP functional with the 6-31G(d) basis set [32] and Grimme's three-parameter which is an empirical dispersion correction [33]. Here, the main reason to use the B3LYP is that it agrees perfectly with the experimental values for the ZnO NCs [34, 35], so the B3LYP was used to study electronic structure of the studied system in this study. To get the possible interactions of the favipiravir drug molecule with ZnO NCs, the favipiravir and ZnO NCs, firstly, were optimized, and later, the structures with the lowest total energy (E_T) were considered. All calculations were carried out using Gaussian 09 [36]. To calculate the adsorption energy (E_{ad}) of favipiravir drug and ZnO NCs interactions, the following expression is used:

$$E_{ad} = E(NC + Drug) - E(NC) - E(Drug) + E(BSSE) \quad (1)$$

where $E(NC + Drug)$ is the total energy (E_T) of the interacting systems. $E(NC)$ and $E(Drug)$ are the E_T of isolated NCs and favipiravir, respectively. $E(BSSE)$ is known as the "basis set superposition error," which is calculated by the counterpoise method to obtain highly accurate energy prediction [37].

On the other hand, the vertical ionization potential (*VIP*) and vertical electron affinity (*VEA*) are performed using $[VIP = E^{cation} - E^{neutral}]$ and $[VEA = E^{neutral} - E^{anion}]$ where the *VIP* is the energy difference between the ground state (*GS*) of the cation $\left(E^{cation}\right)$ and the *GS* of the neutral $\left(E^{neutral}\right)$ at the geometry of the neutral. *VEA* is the energy difference between the *GS* of the neutral and the *GS* of the anion $\left(E^{anion}\right)$ at the geometry of the neutral. Moreover, the Wiberg bond index (WBI), Fuzzy bond orders (FBO), and Mayer bond order (MBO) are performed using the Multiwfn program [38]. The TD-DFT calculations based on CAM-B3LYP functional [39] with 6-31G(d) basis set are applied for guessing UV–vis spectra.

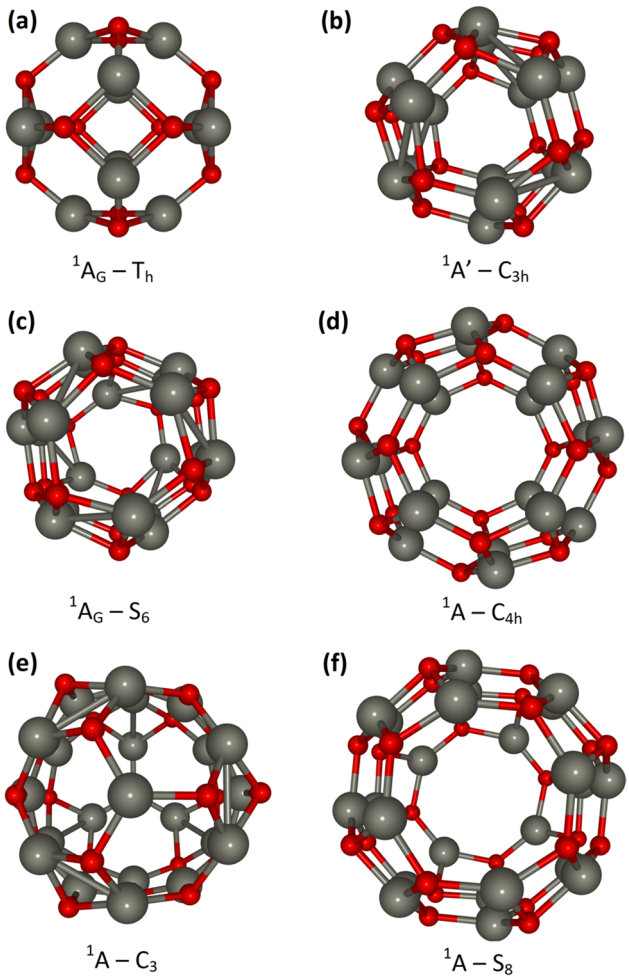

Fig. 1 (Color online) The optimized structures, electronic states, and point group symmetries of pure **a** $(ZnO)_{12}$, **b** $(ZnO)_{15}$, **c** $(ZnO)_{18}$, **d** $(ZnO)_{20}$, **e** $(ZnO)_{22}$, and **f** $(ZnO)_{24}$ NCs (Gray: Zn, Red: O)

Results and discussions

The structures, electronic states, and point group symmetries of pure $(ZnO)_{12}$, $(ZnO)_{15}$, $(ZnO)_{18}$, $(ZnO)_{20}$, $(ZnO)_{22}$, and $(ZnO)_{24}$ NCs are optimized and represented in Fig. 1. The $(ZnO)_{12}$ and $(ZnO)_{18}$ NCs are found to be the potential energy surface (PES) of the ^1A_G state, and the $(ZnO)_{15}$ NC is the ground $^1A'$ singlet PES. The $(ZnO)_{20}$, $(ZnO)_{22}$, and $(ZnO)_{24}$ NCs are found to be the PES of the ^1A state. The point group symmetries of $(ZnO)_{12}$, $(ZnO)_{15}$, $(ZnO)_{18}$, $(ZnO)_{20}$, $(ZnO)_{22}$, and $(ZnO)_{24}$ NCs are T_h, C_{3h}, S_6, C_{4h}, C_3, and S_8, respectively. From the harmonic vibrational frequencies, the studied ZnO NC models corresponded to energetic minimum which means the transition state at a saddle point on the PES.

All possible interactions of the $(ZnO)_{12}$, $(ZnO)_{15}$, $(ZnO)_{18}$, $(ZnO)_{20}$, $(ZnO)_{22}$, and $(ZnO)_{24}$ NCs with favipiravir drug were carried out, and among them, relaxed structures with the lowest energy are demonstrated in Fig. 2. The binding energy per atom (E_b) of pure ZnO NCs and adsorption energy (E_{ad}) of theoretically calculated geometries of the favipiravir adsorbed ZnO NCs are depicted in Fig. 3. The E_b of the ZnO NCs shifts from 5.04 to 5.16 eV, depending on the increase in the size. These results indicate that an increase in the size of the NCs also enhances the stability.

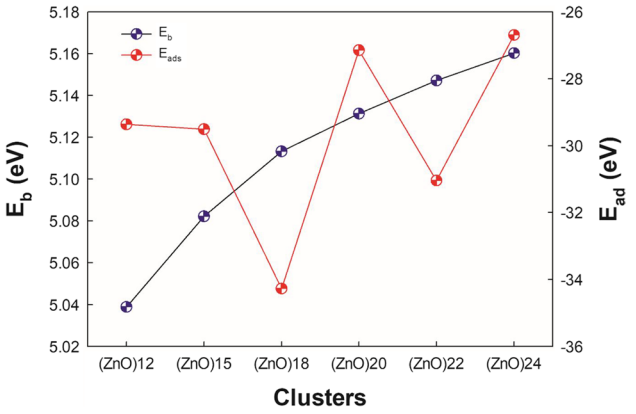

Fig. 3 (Color online) Binding energy per atom (E_b) of pure ZnO clusters and adsorption energy (E_{ad}) for favipiravir adsorbed ZnO NCs

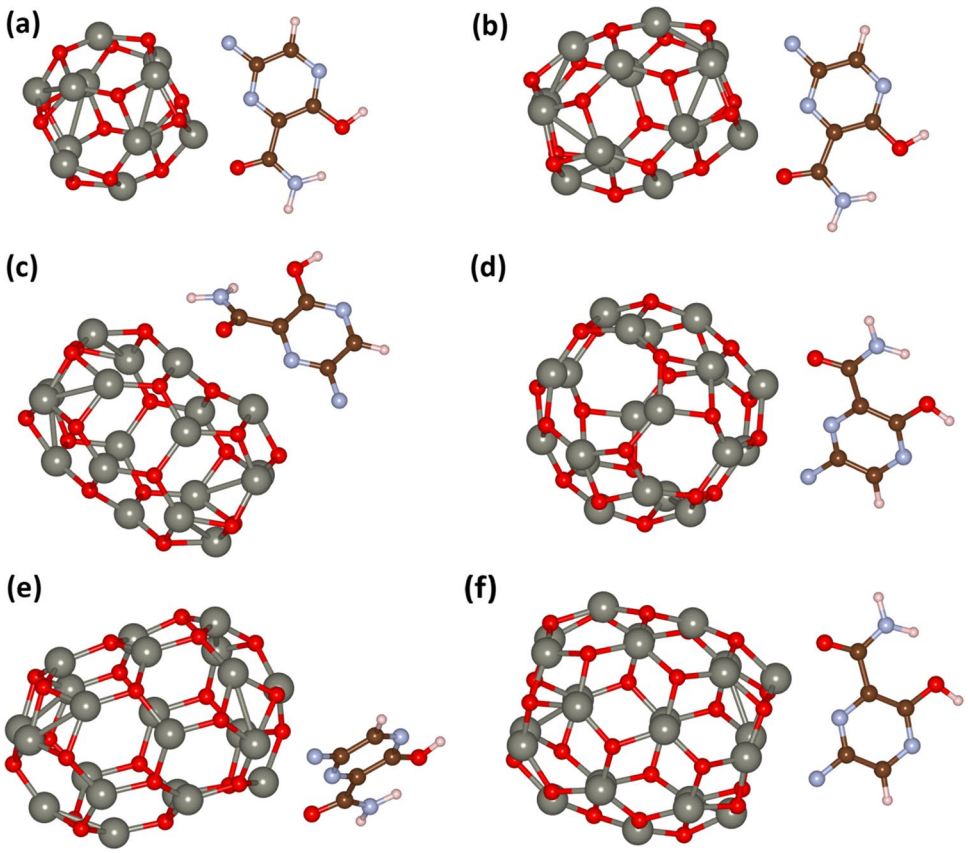

Fig. 2 (Color online) Relaxed structures for favipiravir adsorbed **a** $(ZnO)_{12}$, **b** $(ZnO)_{15}$, **c** $(ZnO)_{18}$, **d** $(ZnO)_{20}$, **e** $(ZnO)_{22}$, and **f** $(ZnO)_{24}$ NCs

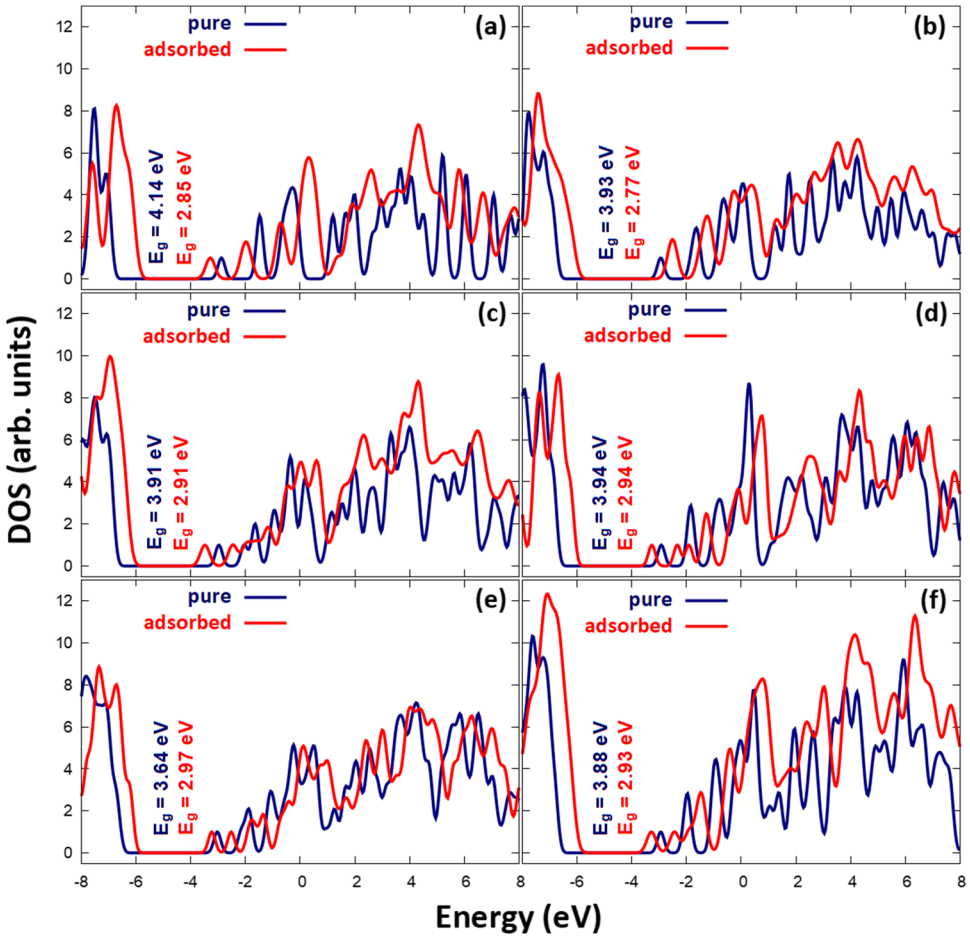

Fig. 4 (Color online) Density of states (DOS) for pure and favipiravir adsorbed **a** $(ZnO)_{12}$, **b** $(ZnO)_{15}$, **c** $(ZnO)_{18}$, **d** $(ZnO)_{20}$, **e** $(ZnO)_{22}$, and **f** $(ZnO)_{24}$ NCs

Table 1 The calculated binding energy per atom (E_b), adsorption energy (E_{ad}), vertical ionization potential (VIP), vertical electron affinity (VEA), HOMO and LUMO energies, band gap energy (E_g), and reactivity parameters for pure and favipiravir adsorbed ZnO NCs. E_{ad} in kcal/mol. Electronic properties are described in eV

	$(ZnO)_{12}$		$(ZnO)_{15}$		$(ZnO)_{18}$		$(ZnO)_{20}$		$(ZnO)_{22}$		$(ZnO)_{24}$	
	Pure	Ads	Pure	Ads	Pure	Ads	Pure	Ads	Pure	Ads	Pure	Ads
E_b	5.04	-	5.08	-	5.11	-	5.13	-	5.15	-	5.16	-
E_{ad}	-	−29.36	-	−29.50	-	−34.27	-	−27.14	-	−31.04	-	−26.69
VIP	8.40	7.46	8.13	7.29	8.03	7.53	7.99	7.31	7.80	7.25	7.84	7.25
VEA	1.64	1.57	1.79	1.67	1.90	1.95	1.87	1.76	2.01	1.86	1.97	1.85
LUMO	−2.86	−3.27	−2.92	−3.28	−2.96	−3.47	−2.90	−3.25	−3.01	−3.22	−2.92	−3.27
HOMO	−7.00	−6.12	−6.85	−6.05	−6.87	−6.38	−6.84	−6.19	−6.65	−6.19	−6.80	−6.20
E_g	4.14	2.85	3.93	2.77	3.91	2.91	3.94	2.94	3.64	2.97	3.88	2.93
ΔE_g (%)*	-	31.16	-	29.52	-	25.58	-	25.38	-	18.41	-	24.48
η	2.07	1.43	1.97	1.39	1.96	1.46	1.97	1.47	1.82	1.49	1.94	1.47
ΔN_{tot}	2.38	3.29	2.49	3.37	2.51	3.38	2.47	3.21	2.65	3.17	2.51	3.23

*ΔE_g (%) denotes the changes after adsorption

The E_{ad} of the ZnO NCs is predicted in the range of − 26.69 and − 34.27 kcal/mol where N–Zn and F–Zn atoms interact between the N and F atoms of favipiravir drug and Zn atoms of the ZnO NCs. The negative E_{ad} means that the adsorption of the favipiravir drug on ZnO NCs is exothermic and energetically favorable. The size of ZnO NC has a significant effect on the E_{ad} between the favipiravir and ZnO NCs. It is important to note that the E_{ad} (− 34.27 kcal/mol) of between $(ZnO)_{18}$ NC and the favipiravir is more desirable than the other interactions $(ZnO)_{24}$ (− 26.69 kcal/mol), $(ZnO)_{20}$ (− 27.14 kcal/mol), $(ZnO)_{12}$ (− 29.36 kcal/mol), $(ZnO)_{15}$ (− 29.50 kcal/mol), and $(ZnO)_{22}$ (− 31.04 kcal/mol) NCs with the favipiravir, which means that ZnO NCs can be used as drug delivery vehicle.

The HOMO and LUMO energy levels are important parameters to understand perfectly the charge transfer interaction within interacting systems [40]. In this regard, the energy levels using the density of states (DOS) constructed by GaussSum [41] (Fig. 4) and the energy gap (E_g) that is obtained from HOMO and LUMO energy differences are performed to figure out the stability chemical reaction of the studied systems. The size of ZnO NCs causes changes over valence and conduction levels to shift to higher and lower energies both pure and interacting systems, leading to a shift in the studied systems. Our DFT calculations reveal that the E_g of $(ZnO)_{12}$, $(ZnO)_{15}$, $(ZnO)_{18}$, $(ZnO)_{20}$, $(ZnO)_{22}$, and $(ZnO)_{24}$ NCs is found to be 4.14, 3.93, 3.91, 3.94, 3.64, and 3.88 eV, respectively (Table 1). Compared to studies available in the literature, the E_g of $(ZnO)_{12}$ was predicted as 4.04 eV [21] wide, i.e., about 0.10 eV smaller than the calculated E_g value in the considered ZnO NC in this study. To the best of our knowledge, the other structures (for $n = 15$, 18, 20, 22, and 24) studied in the literature are cage structures [42, 43], but they are not symmetric as in our study, so these structures did not compare with our structures, just cited in References [21] and [42].

The value of the HOMO and LUMO energy levels is found to be about − 6.05 and − 3.28 eV, respectively, and the corresponding E_g is found as 2.77 eV for $(ZnO)_{15}$ NC and the favipiravir interaction which is the smallest value among the studied models. Moreover, the HOMO and LUMO energy levels for $(ZnO)_{12}$ NC and the favipiravir interaction are predicted as − 6.19 and − 3.25 eV, respectively. The corresponding E_g is found to be 2.94 eV, which is greater than the other ZnO NC, and the favipiravir interactions change

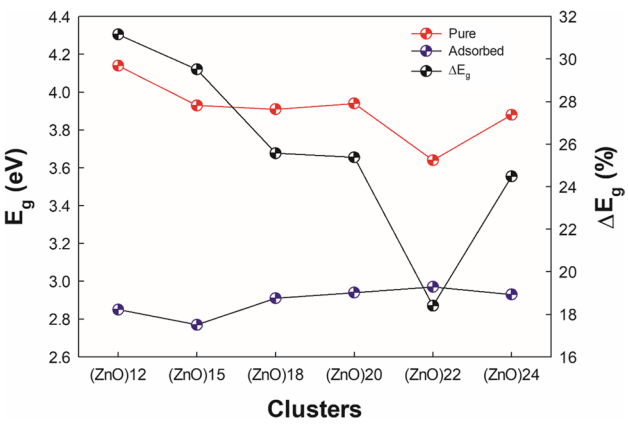

Fig. 5 (Color online) The HOMO–LUMO energy gap (E_g) and the percentage value (ΔE_g) of the difference in the E_g energies for pure and favipiravir adsorbed ZnO NCs

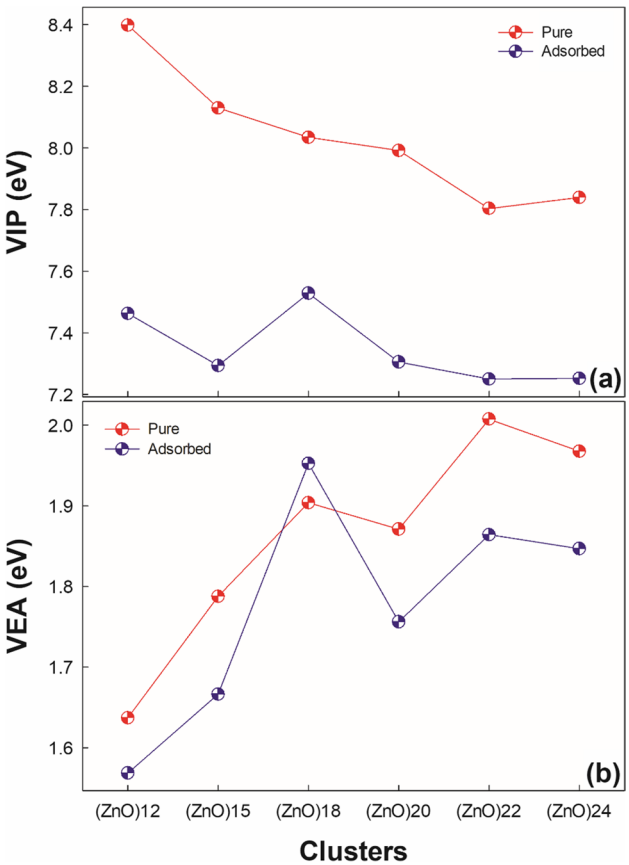

Fig. 6 (Color online) **a** VIP and **b** VEA for pure and favipiravir adsorbed ZnO NCs

in the range of 2.85–3.94 eV. It is important to note that charge transfer can take place easier between HOMO and LUMO energy levels of $(ZnO)_{15}$ NC which has the smallest E_g value and the favipiravir interaction, which means a shift in the biological activity of the favipiravir and ZnO NC interaction as shown in Fig. 5. That is, the change in the size of the ZnO NCs and the position of the favipiravir on the ZnO NCs cause a desirable shift in the HOMO and LUMO energy levels due to a decrease in the E_g, which further contributes to the charge-transfer process [44–46]. The percentage value $\left(\Delta E_g\right)$ of the difference in the E_g energies for favipiravir adsorbed ZnO NCs is also given in Fig. 5. When compared to pure ZnO NCs, the greatest change in the ΔE_g is predicted between $(ZnO)_{12}$ NC and favipiravir (31.16%), whereas the lowest change in the ΔE_g is predicted between $(ZnO)_{22}$ NC and favipiravir (18.41%). The values show that the size of ZnO NCs has an important effect on the E_g of interactions. The ZnO NCs are semi-conducting with the E_g in the range of 2.77–2.97 eV.

The vertical ionization potential (VIP) and vertical electron affinity (VEA), which are defined in computational part, are carried out to explore the changes of the reactivity properties of pure ZnO NCs and ZnO NCs with favipiravir drug based on the size of ZnO NCs, as indicated in Fig. 6a, b. The greater *VIP* value of pure $(ZnO)_{12}$ NC is 8.40 eV, which decreases to 7.84 eV for $(ZnO)_{24}$ NC due to the increase in HOMO and LUMO energy levels in terms of the electron-donating ability of the favipiravir towards ZnO NCs. Similarly, the greater *VIP* value of $(ZnO)_{18}$ NC with favipiravir drug is 7.53 eV, which decreases to 7.25 eV for $(ZnO)_{22}$ and $(ZnO)_{24}$ NCs with favipiravir drug as shown in Fig. 6a. It is important to note that pure $(ZnO)_{12}$ NC and $(ZnO)_{18}$ NC with favipiravir drug are more stable than that of the others, so it is difficult to eject the electron from them.

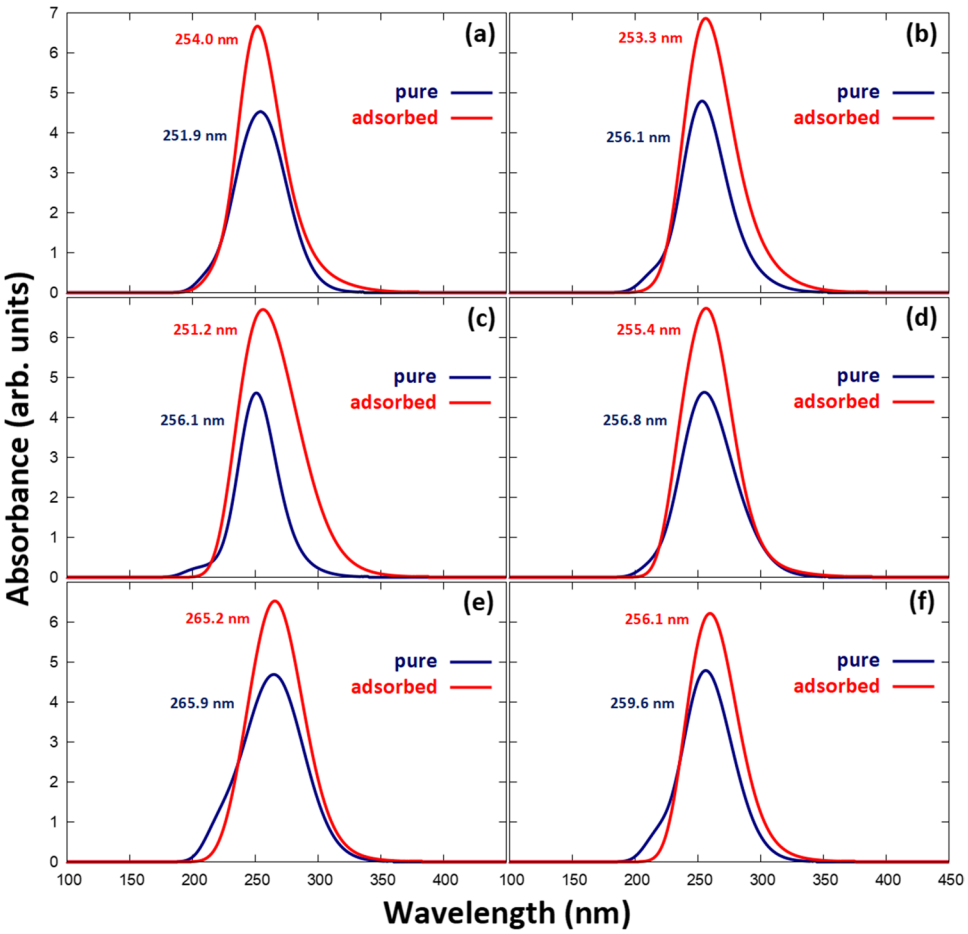

Fig. 7 (Color online) UV–vis spectra for pure and favipiravir adsorbed **a** $(ZnO)_{12}$, **b** $(ZnO)_{15}$, **c** $(ZnO)_{18}$, **d** $(ZnO)_{20}$, **e** $(ZnO)_{22}$, and **f** $(ZnO)_{24}$ NCs

Table 2 Bond orders (Wiberg bond index (WBI), Fuzzy bond order (FBO), Mayer bond order (MBO)) and Mulliken charges based on interactions between O–Zn, N–Zn, and F–Zn atoms (The O, N, and F atoms indicate favipiravir; the Zn is the closest neighbors to these atoms; see Supporting information Fig. S1 for detail)

Configurations	Interactions	WBI	FBO	MBO	Charge
Drug–$(ZnO)_{12}$	27O–19Zn	0.414	0.732	0.363	0.321
	35 N–19Zn	0.189	0.369	0.115	0.072
	34F–6Zn	0.056	0.105	0.072	0.064
Drug–$(ZnO)_{15}$	33O–30Zn	0.415	0.732	0.365	0.325
	41 N–30Zn	0.195	0.378	0.117	0.074
	40F–7Zn	0.031	0.041	0.042	0.039
Drug–$(ZnO)_{18}$	39O–25Zn	0.370	0.675	0.334	0.304
	47 N–9Zn	0.373	0.636	0.259	0.241
	46F–9Zn	0.042	0.079	0.087	0.085
Drug–$(ZnO)_{20}$	43O–19Zn	0.426	0.750	0.409	0.358
	51 N–19Zn	0.089	0.167	0.061	0.061
	50F–16Zn	0.145	0.312	0.187	0.169
Drug–$(ZnO)_{22}$	47O–33Zn	0.432	0.762	0.402	0.360
	55 N–33Zn	0.067	0.119	0.029	0.033
	54F–25Zn	0.175	0.371	0.229	0.199
Drug–$(ZnO)_{24}$	51O–16Zn	0.405	0.725	0.370	0.338
	59 N–16Zn	0.172	0.338	0.092	0.053
	58F–22Zn	0.041	0.060	0.045	0.040

This result agrees also with the energy levels of HOMO and LUMO (Table 1). The VIP of the $(ZnO)_{15}$, $(ZnO)_{18}$, and $(ZnO)_{20}$ NCs with favipiravir drug is predicted as 7.29, 7.53, and 7.31 eV. The value of *VEA* of pure $(ZnO)_{20}$ is 2.01 eV, which decreases to 1.64 eV for pure $(ZnO)_{20}$ as shown in Fig. 6b. Similarly, the greater *VEA* value of $(ZnO)_{18}$ NC with favipiravir drug is 1.95 eV, which decreases to 1.57 eV for $(ZnO)_{12}$ NC with favipiravir drug as shown in Fig. 6b. There is not a smooth change for the *VEA* with increase in the size of ZnO NC where the value of *VEA* increases for $(ZnO)_{12}$, $(ZnO)_{15}$, and $(ZnO)_{18}$ with the favipiravir drug from 1.64 to 1.95 eV, and then fluctuations are observed from $(ZnO)_{20}$ to $(ZnO)_{24}$ with the favipiravir drug.

Ultraviolet–visible (UV–vis) absorption spectra of interacting pure and favipiravir adsorbed $(ZnO)_{12}$, $(ZnO)_{15}$, $(ZnO)_{18}$, $(ZnO)_{20}$, $(ZnO)_{22}$, $(ZnO)_{24}$ NCs are performed with TD-DFT, and the obtained results are piloted in Fig. 7. An excitation wavelength (electron-transfer wavelength) in the visible region is preferred because ultraviolet light is harmful to living organisms [47]. Our results show that maximum absorption wavelength between 250 and 265 nm was obtained for interacting ZnO NCs and favipiravir systems,

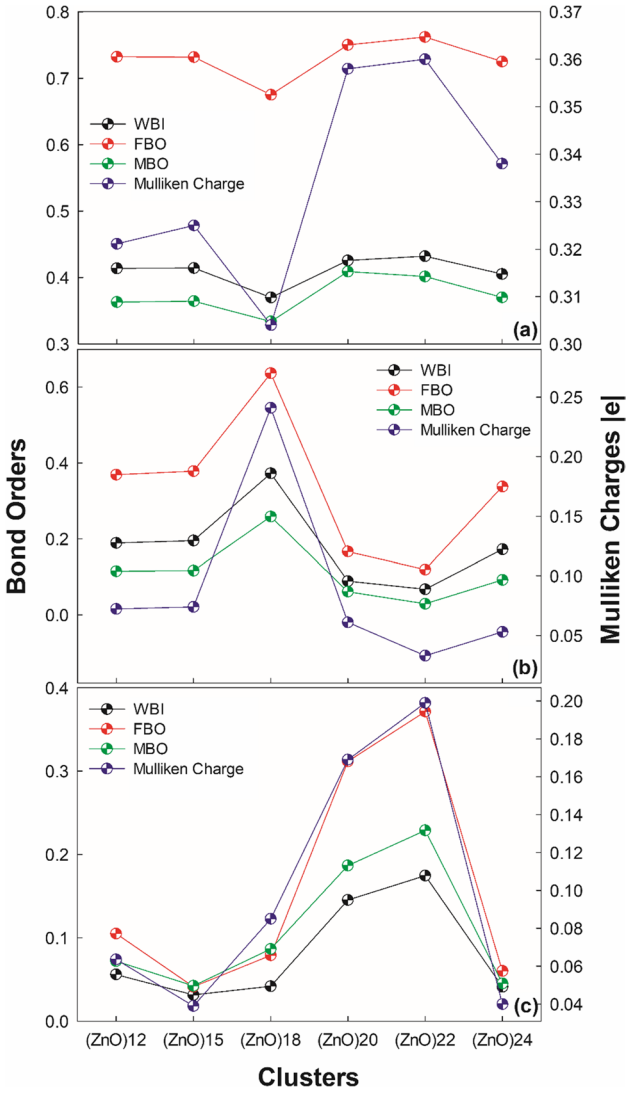

Fig. 8 (Color online) Wiberg bond index (WBO), Mayer bond order (MBO), and Fuzzy bond order (FBO) and Mulliken charges based on interactions between **a** O–Zn, **b** N–Zn, and **c** F–Zn atoms for favipiravir adsorbed ZnO NCs (O, N, and F atoms indicate favipiravir and Zn indicates ZnO NCs; according to Supporting information Fig. S1 for detail)

which corresponds to the near UV region and the closest visible light.

The bond order analysis of ZnO NCs with different sizes and favipiravir interactions was studied using WBO, MBO, and FBO methods. The values of WBI, FBO, and MBO for the favipiravir on the $(ZnO)_{22}$ NC were calculated about 0.432, 0.762, and 0.402, respectively, which are greater than other configurations (Table 2, Fig. 8, and Fig. S1 in the Supporting information). WBI, FBO, and

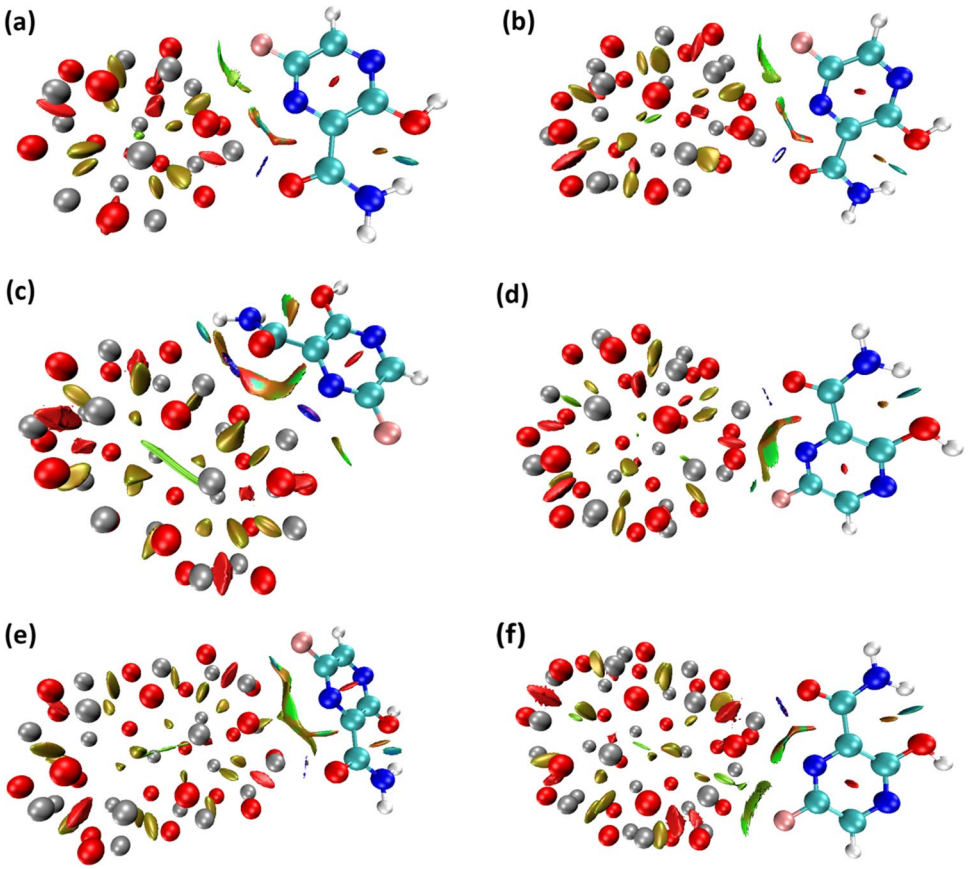

Fig. 9 (Color online) The non-covalent interaction (NCI) isosurfaces for favipiravir adsorbed **a** $(ZnO)_{12}$, **b** $(ZnO)_{15}$, **c** $(ZnO)_{18}$, **d** $(ZnO)_{20}$, **e** $(ZnO)_{22}$, and **f** $(ZnO)_{24}$ NCs

MBO values also vary considerably based on the NC size and binding points of favipiravir molecule. Bond order values below 1.0 reflect the fact that bonds between O–Zn, N–Zn, and F–Zn atoms exhibit dual covalent and ionic natures. Besides, the presence of metal ions bonded to oxygen atoms means that the O–Zn bonds are kind of polarized covalent bonds. The Mulliken charge distribution of the atoms in the ZnO NCs with different sizes and favipiravir interactions is also tabulated in Table 2 and shown in Fig. S1 (in the Supporting information). As can be seen from Table 2, the charges on the O–Zn interactions have been calculated between 0.304 and 0.360 lel, which are significantly bigger than that of N–Zn and F–Zn interactions.

To get an insight into the non-covalent interactions (NCI) within the studied systems, the NCI isosurfaces for favipiravir adsorbed $(ZnO)_{12}$, $(ZnO)_{15}$, $(ZnO)_{18}$, $(ZnO)_{20}$, $(ZnO)_{22}$, and $(ZnO)_{24}$ NCs are investigated, and plots for studied systems are shown in Fig. 9. As can be seen, disk-shaped blocks that indicate non-covalent interactions and the strongest H-bonds are observed near NH_2 within the favipiravir molecule. Furthermore, the reduced density gradient (RDG) scatter plots for favipiravir adsorbed ZnO NCs were presented in Fig. 10. RDG scattered points indicate H-bonding interactions on the negative scale (blue color), indicating the dominance of the effect of strong attractive interactions. The green region in the range of $\rho = 0.00$ and $\rho = -0.02$ also shows the dominance of the effect of Van der Waals forces between binding atoms. Red areas indicate strong repulsive/steric interactions in a range of 0.01 and 0.05.

Conclusions

In this study, the adsorption behavior and electronic and structural properties of the interacting favipiravir drug and ZnO NCs with different sizes were determined using the DFT method. Our results show the size of ZnO NCs, and binding points have an important effect on the interactions. For example, the adsorption energy between $(ZnO)_{18}$ NC and the favipiravir (− 34.27 kcal/mol) is energetically more favorable than the other interactions. The size of the ZnO NCs causes a decrease in the energy gap, which further contributes to the charge-transfer process. The bonds between O–Zn, N–Zn, and F–Zn atoms exhibit dual covalent and ionic natures.

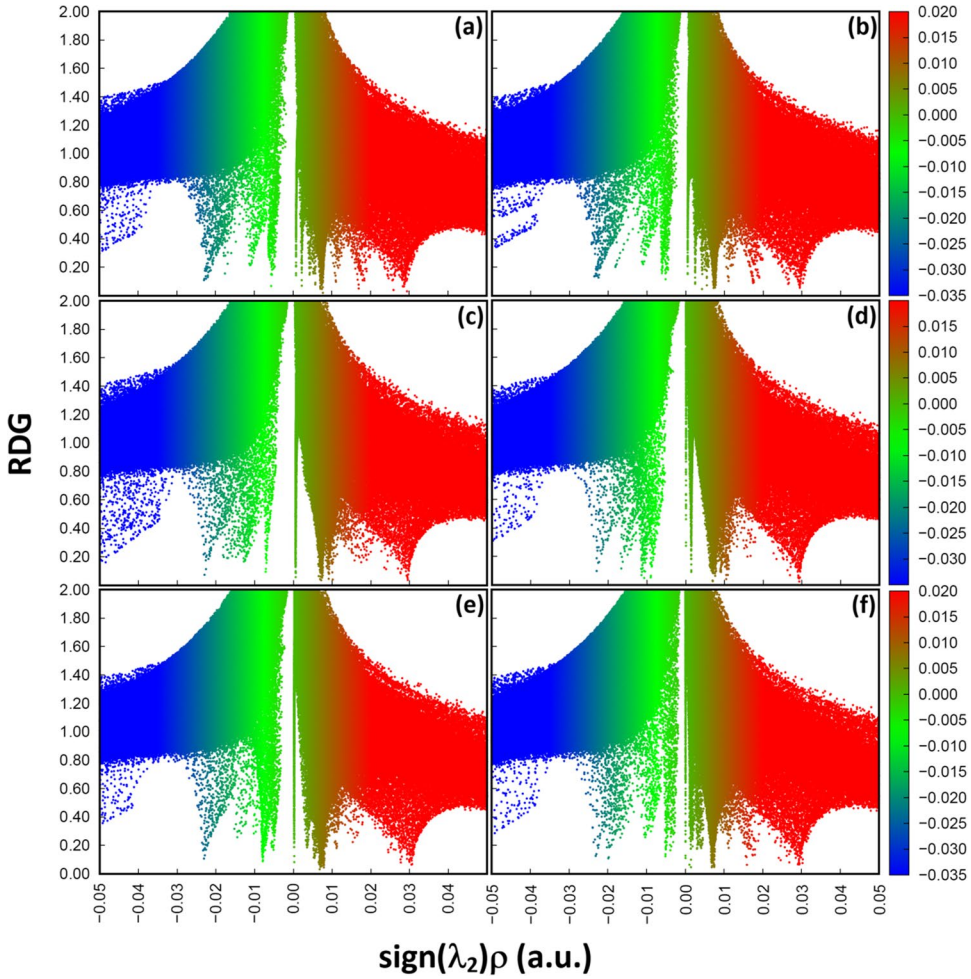

Fig. 10 (Color online) The reduced density gradient (RDG) scatter plots for favipiravir adsorbed **a** $(ZnO)_{12}$, **b** $(ZnO)_{15}$, **c** $(ZnO)_{18}$, **d** $(ZnO)_{20}$, **e** $(ZnO)_{22}$, and **f** $(ZnO)_{24}$ NCs. Blue represents strong attractive interactions; green indicates van der Waals interactions; and red indicates repulsive/steric interactions

From the non-covalent interaction analysis, the strongest H-bonds are observed near NH_2 within the favipiravir. The maximum absorption peaks are predicted in the near UV region and the closest visible light. We can conclude that the ZnO NCs can have potential as drug delivery carriers.

Supplementary Information The online version contains supplementary material available at https://doi.org/10.1007/s11224-022-02063-2.

Acknowledgements The numerical calculations reported were partially performed at TUBITAK ULAKBIM, High Performance and Grid Computing Centre (TRUBA resources), Turkey.

Author contribution Mustafa Kurban: supervision, investigation, conceptualization, writing—original draft, writing—review and editing, data curation, validation, and software.

İskender Muz: investigation, project administration, visualization, methodology, conceptualization, writing—original draft, writing—review and editing, data curation, and software.

Research data policy and data availability Data sharing not applicable to this article as no datasets were generated or analyzed during the current study.

Declarations

Ethics approval This article does not contain any studies involving human participants performed by any of the authors.

Competing interests The authors declare no competing interests.

References

1. Wager J, Yeh B, Hoffman R et al (2014) An amorphous oxide semiconductor thin-film transistor route to oxide electronics. Curr Opin Solid State Mater Sci 18:53–61
2. Laurenti M, Canavese G, Stassi S et al (2016) A porous nanobranched structure: an effective way to improve piezoelectricity in sputtered ZnO thin films. RSC Adv 6:76996–77004
3. Liu J, Fernández-Serra MV, Allen PB (2016) First-principles study of pyroelectricity in GaN and ZnO. Phys Rev B 93:081205. https://doi.org/10.1103/PhysRevB.93.081205
4. Song RQ, Xu AW, Deng B et al (2007) From layered basic zinc acetate nanobelts to hierarchical zinc oxide nanostructures and porous zinc oxide nanobelts. Adv Funct Mater 17:296–306. https://doi.org/10.1002/ADFM.200600024

5. Hu P, Liu Y, Wang X et al (2003) Tower-like structure of ZnO nanocolumns. Chem Commun 11:1304–1305. https://doi.org/10.1039/B302821F
6. Zhang J, Sun L, Liao C, Yan C (2002) A simple route towards tubular ZnO. Chem Commun 2:262–263. https://doi.org/10.1039/B108863G
7. Polarz S, Orlov A V, Schüth F et al (2007) Preparation of high-surface-area zinc oxide with ordered porosity, different pore sizes, and nanocrystalline walls. Chem Eur J 13:592–597. https://doi.org/10.1002/chem.200600428
8. Kong XY, Ding Y, Yang R, Wang ZL (2004) Single-crystal nanorings formed by epitaxial self-coiling of polar nanobelts. Science (80) 303:1348–1351
9. Zhong X, Knoll W (2005) Morphology-controlled large-scale synthesis of ZnO nanocrystals from bulk ZnO. Chem Commun 2005:1158–1160. https://doi.org/10.1039/B414948C
10. Chang S-P, Chen K-J (2012) Zinc oxide nanoparticle photodetector. J Nanomater 2012:1–5. https://doi.org/10.1155/2012/602398
11. Kołodziejczak-Radzimska A, Jesionowski T (2014) Zinc oxide—From synthesis to application: a review. Materials (Basel) 7:2833–2881. https://doi.org/10.3390/ma7042833
12. Zhang Y, Nayak T, … HH-C molecular, 2013 U (2013) Biomedical applications of zinc oxide nanomaterials. Curr Mol Med 13:1633–1645
13. Rasmussen JW, Martinez E, Louka P, Wingett DG (2010) Zinc oxide nanoparticles for selective destruction of tumor cells and potential for drug delivery applications. Expert Opin Drug Deliv 7:1063–1077. https://doi.org/10.1517/17425247.2010.502560
14. Xiong H-M, Xiong H-M (2013) ZnO nanoparticles applied to bioimaging and drug delivery. Adv Mater 25:5329–5335. https://doi.org/10.1002/ADMA.201301732
15. Saha S, Sarkar P (2014) Understanding the interaction of DNA-RNA nucleobases with different ZnO nanomaterials. Phys Chem Chem Phys 16:15355–15366. https://doi.org/10.1039/C4CP01041H
16. Chandraboss VL, Karthikeyan B, Senthilvelan S (2014) Experimental and first-principles study of guanine adsorption on ZnO clusters. Phys Chem Chem Phys 16:23461–23475. https://doi.org/10.1039/C4CP03274H
17. Yang X, Zhang X, Liu Z et al (2008) High-efficiency loading and controlled release of doxorubicin hydrochloride on graphene oxide. J Phys Chem C 112:17554–17558. https://doi.org/10.1021/JP806751K
18. Rosli NF, Fojtů M, Fisher AC, Pumera M (2019) Graphene oxide nanoplatelets potentiate anticancer effect of cisplatin in human lung cancer cells. Langmuir 35:3176–3182. https://doi.org/10.1021/ACS.LANGMUIR.8B03086
19. Baek M, Chung HE, Yu J et al (2012) Pharmacokinetics, tissue distribution, and excretion of zinc oxide nanoparticles. Int J Nanomedicine 7:3081. https://doi.org/10.2147/IJN.S32593
20. Choi SJ, Choy JH (2014) Biokinetics of zinc oxide nanoparticles: toxicokinetics, biological fates, and protein interaction. Int J Nanomedicine 9:261. https://doi.org/10.2147/IJN.S57920
21. Xu W, Cao H, Chen H et al (2021) Sensing the cathinone drug concentration in the human body by using zinc oxide nanostructures: a DFT study. Struct Chem 32:63–68. https://doi.org/10.1007/s11224-020-01611-y
22. Ji X, Jameh-Bozorghi S (2020) Metal oxide nanoclusters as drug delivery systems for an anticancer drug: a theoretical study. Mol Phys 118:e1738581. https://doi.org/10.1080/00268976.2020.1738581
23. Bai L, Li X, He L et al (2019) Antidiabetic potential of flavonoids from traditional Chinese medicine: a review. Am J Chin Med 47:933–957. https://doi.org/10.1142/S0192415X19500496
24. Sharma P, Scott DGI (2015) Optimizing methotrexate treatment in rheumatoid arthritis: the case for subcutaneous methotrexate prior to biologics. Drugs 75:1953–1956. https://doi.org/10.1007/s40265-015-0486-7
25. Kurban M, Muz İ (2020) Theoretical investigation of the adsorption behaviors of fluorouracil as an anticancer drug on pristine and B-, Al-, Ga-doped C36 nanotube. J Mol Liq 309:113209. https://doi.org/10.1016/j.molliq.2020.113209
26. Khezri B, Beladi Mousavi SM, Krejčová L et al (2019) Ultrafast electrochemical trigger drug delivery mechanism for nanographene micromachines. Adv Funct Mater 29:1806696. https://doi.org/10.1002/adfm.201806696
27. Campuzano S, Esteban-Fernández De Ávila B, Yáñez-Sedeño P et al (2017) Nano/microvehicles for efficient delivery and (bio) sensing at the cellular level. Chem Sci 8:6750–6763. https://doi.org/10.1039/c7sc02434g
28. Sham LJ, Kohn W (1966) One-particle properties of an inhomogeneous interacting electron gas. Phys Rev 145:561–567. https://doi.org/10.1103/PHYSREV.145.561
29. Wang M, Cao R, Zhang L et al (2020) Remdesivir and chloroquine effectively inhibit the recently emerged novel coronavirus (2019-nCoV) in vitro. Cell Res 30:269–271. https://doi.org/10.1038/S41422-020-0282-0
30. De Clercq E (2019) New nucleoside analogues for the treatment of hemorrhagic fever virus infections. Chem Asian J 14:3962. https://doi.org/10.1002/ASIA.201900841
31. Yao C, Xiang F, Xu Z (2022) Metal oxide nanocage as drug delivery systems for favipiravir, as an effective drug for the treatment of COVID-19: a computational study. J Mol Model 28:64. https://doi.org/10.1007/s00894-022-05054-6
32. Becke AD (1993) A new mixing of hatree-fock and local density functional theories. J Chem Phys 98:1372–1377. https://doi.org/10.1063/1.464304
33. Grimme S, Ehrlich S, Goerigk L (2011) Effect of the damping function in dispersion corrected density functional theory. J Comput Chem 32:1456–1465. https://doi.org/10.1002/jcc.21759
34. Aljawfi RN, Alam MJ, Rahman F et al (2020) Impact of annealing on the structural and optical properties of ZnO nanoparticles and tracing the formation of clusters via DFT calculation. Arab J Chem 13:2207–2218. https://doi.org/10.1016/j.arabjc.2018.04.006
35. Muz İ, Kurban M (2022) Zinc oxide nanoclusters and their potential application as CH4 and CO2 gas sensors: insight from DFT and TD-DFT. J Comput Chem n/a:1–9. https://doi.org/10.1002/jcc.26986
36. Gaussian 09, Revision E.01, Frisch, MJ, Trucks GW, Schlegel HB, Scuseria GE, Robb MA, Cheeseman JR, Scalmani G, Barone V, Mennucci B, Petersson GA, Nakatsuji H, Caricato M, Li X, Hratchian HP, Izmaylov AF, Bloino J, Zheng G, Sonnenberg JL, Hada M, Ehara M, Toyota K, Fukuda R, Hasegawa J, Ishida M, Nakajima T, Honda Y, Kitao O, Nakai H, Vreven T, Montgomery JA Jr., Peralta JE, Ogliaro F, Bearpark M, Heyd JJ, Brothers E, Kudin KN, Staroverov VN, Kobayashi R, Normand J, Raghavachari K, Rendell A, Burant JC, Iyengar SS, Tomasi J, Cossi M, Rega N, Millam JM, Klene M, Knox JE, Cross JB, Bakken V, Adamo C, Jaramillo J, Gomperts R, Stratmann RE, Yazyev O, Austin AJ, Cammi R, Pomelli C, Ochterski JW, Martin RL, Morokuma K, Zakrzewski VG, Voth GA, Salvador P, Dannenberg JJ, Dapprich S, Daniels AD, Farkas Ö, Foresman JB, Ortiz JV, Cioslowski J, Fox DJ, Gaussian Inc., Wallingford CT (2009)
37. Boys SF, Bernardi F (1970) The calculation of small molecular interactions by the differences of separate total energies. Some procedures with reduced errors. Mol Phys 19:553–566. https://doi.org/10.1080/00268977000101561

38. Lu T, Chen F (2012) Multiwfn: a multifunctional wavefunction analyzer. J Comput Chem 33:580–592. https://doi.org/10.1002/jcc.22885
39. Yanai T, Tew DP, Handy NC (2004) A new hybrid exchange–correlation functional using the Coulomb-attenuating method (CAM-B3LYP). Chem Phys Lett 393:51–57. https://doi.org/10.1016/j.cplett.2004.06.011
40. Zaboli M, Raissi H (2015) The analysis of electronic structures, adsorption properties, NBO, QTAIM and NMR parameters of the adsorbed hydrogen sulfide on various sites of the outer surface of aluminum phosphide nanotube: a DFT study. Struct Chem 26:1059–1075. https://doi.org/10.1007/s11224-015-0563-2
41. O'Boyle NM, Tenderholt AL, Langner KM (2008) cclib: a library for package-independent computational chemistry algorithms. J Comput Chem 29:839–845. https://doi.org/10.1002/jcc.20823
42. Wang B, Nagase S, Zhao J, Wang G (2007) Structural growth sequences and electronic properties of zinc oxide clusters (ZnO)n (n=2-18). J Phys Chem C 111:4956–4963. https://doi.org/10.1021/JP066548V
43. Nagare BJ, Chavan S, Bambole V (2017) Study of electronic and optical properties of ZnO clusters using TDDFT method. Mater Res Express 4:106304. https://doi.org/10.1088/2053-1591/aa91e1
44. Salem MA, Katin KP, Kaya S et al (2020) Interaction of dopants and functional groups adsorbed on the carbon fullerenes: computational study. Phys E Low-dimensional Syst Nanostructures 124:114319. https://doi.org/10.1016/j.physe.2020.114319
45. Abdullah NR, Rashid HO, Kareem MT et al (2020) Effects of bonded and non-bonded B/N codoping of graphene on its stability, interaction energy, electronic structure, and power factor. Phys Lett A 384:126350. https://doi.org/10.1016/j.physleta.2020.126350
46. Abdullah NR, Rashid HO, Tang C-S et al (2020) Modeling electronic, mechanical, optical and thermal properties of graphene-like BC6N materials: Role of prominent BN-bonds. Phys Lett A 384:126807. https://doi.org/10.1016/j.physleta.2020.126807
47. Burdette SC, Lippard SJ (2001) ICCC34 - golden edition of coordination chemistry reviews. Coordination chemistry for the neurosciences. Coord Chem Rev 216:333–361. https://doi.org/10.1016/S0010-8545(01)00308-3